GÖTTLICHER, S. (1968). *Acta Cryst.* B24, 122-129.
GÖTTLICHER, S. & KNÖCHEL, C. D. (1980). *Acta Cryst.* B36, 1271-1277.
GÖTTLICHER, S. & VEGAS, A. (1988). *Acta Cryst.* B44, 362-367.
HALL, S. R. & STEWART, J. M. (1990). Editors. *XTAL3.0 Users Manual.* Univs. of Western Australia, Australia, and Maryland, USA.
HAMPEL, F. R., RONCHETTI, E. M., ROUSSEEUW, P. J. & STAHEL, W. A. (1986). *Robust Statistics.* New York: Wiley.
HESTER, J. R., MASLEN, E. N., SPADACCINI, N., ISHIZAWA, N. & SATOW, Y. (1993). *Acta Cryst.* Submitted.
MASLEN, E. N., SPADACCINI, N., ITO, T., MARUMO, F. & SATOW, Y. (1993*a*). *Acta Cryst.* Submitted.
MASLEN, E. N., SPADACCINI, N., ITO, T., MARUMO, F. & SATOW, Y. (1993*b*). In preparation.
MASLEN, E. N., STRELTSOV, V. A., STRELTSOVA, N. R., ISHIZAWA, N., MARUMO, F. & SATOW, Y. (1993). *Acta Cryst.* Submitted.
SPADACCINI, N. (1989). Proceedings of CRYSTAL XVI, Lorne, Australia, L6. Society of Crystallographers in Australia.
YAMANE, M. (1973). *Statistics, an Introductory Analysis*, 3rd ed. New York: Harper & Row.
ZACHARIASEN, W. H. (1967). *Acta Cryst.* A23, 558-564.

Acta Cryst. (1993). A49, 667–676

One-Dimensional Quasilattices: Fractally Shaped Atomic Surfaces and Homometry

BY E. ZOBETZ

Institut für Mineralogie, Kristallographie und Strukturchemie, Technische Universität Wien, Getreidemarkt 9, A-1060 Vienna, Austria

(*Received* 17 *June* 1992; *accepted* 1 *February* 1993)

Abstract

The section method was used to determine the atomic surfaces of one-dimensional quasilattices generated by means of deflation rules with the scale factor $\mu=\tau^{-n}$, where $\tau=(1+5^{1/2})/2$ and $1\le n\le 3$. The quasilattices satisfy the condition that the distances between neighboring points take on just the two values of the original Fibonacci quasilattice. Evidence suggests that the atomic surfaces are regular fractals, whose width depends on both length and frequency of periodic inclusions. The frequencies of interpoint distances as well as squared Fourier transforms and simulated diffraction patterns of the quasilattices have been calculated and will be discussed. Generalization of the fractal development of atomic surfaces yields homometric quasicrystals.

1. Introduction

Since the discovery of tiles that force nonperiodic tilings (Penrose, 1974, 1979) and of quasicrystals (Shechtman, Blech, Gratias & Cahn, 1984), much experimental and theoretical work has been focused on the discovery of new types of quasicrystals [for a review the reader is referred to Steurer (1990)] and on several methods for the generation of quasilattices:

(i) deflation procedures (Penrose, 1974, 1979; de Bruijn, 1981; Socolar, 1989);

(ii) grid methods (de Bruijn, 1981; Gähler & Rhyner, 1986; Socolar & Steinhardt, 1986; Korepin, Gähler & Rhyner, 1988);

(iii) the projection and section method (de Bruijn, 1981; Kramer & Neri, 1984; Duneau & Katz, 1985; Kalugin, Kitaev & Levitov, 1985; Elser, 1986; Bak, 1986; Janssen, 1986).

One direction of theoretical research is to increase understanding of the higher-dimensional space-group symmetries (Janner, 1991; Janssen, 1991, 1992). Another direction is to investigate the possibilities of decorating the quasilattices in physical space (Henley, 1986; Kumar, Sahoo & Athithan, 1986) constructed by means of either the projection or the section method. However, surprisingly little attention has been paid to modified window functions (the projection method) or atomic surfaces (the section method) (Zia & Dallas, 1985; Bak, 1986; DiVincenzo, 1986; Elser, 1986). The purpose of this paper is to investigate which kinds of windows (atomic surfaces) correspond to quasilattices obtained by means of 'simple' deflation rules* and what the corresponding effects are on the squared Fourier transforms and diffraction patterns of these quasilattices.

2. Deflation rules

The one-dimensional quasilattices described in this paper have been generated by means of deflation rules with the scale factor $\mu=\tau^{-n}$ $[\tau=(1+5^{1/2})/2]$ with $1\le n\le 3$. They satisfy the condition that the lengths of line segments joining adjacent points take

* 'Simple' deflation rule means that every line segment of a given length is decomposed in the same way.

Table 1. *Deflation of line segments of lengths A and B with the scale factor* $\mu = \tau^{-n}$ $[\tau = (1+5^{1/2})/2, 1 \le n \le 3]$

Each line segment of length A is replaced by F_{n+1} and F_n line segments of lengths A' and B', respectively, and each line segment of length B is replaced by F_n and F_{n-1} line segments of lengths A' and B', respectively, where $F_n = [\tau^n - (-1/\tau)^n]/5^{1/2}$ are the Fibonacci numbers and $A' = \mu A$ and $B' = \mu B$.

n	A	B	Number of combinations
1	$A'B'$	A'	2
	$B'A'$		
2	$A'A'B'$	$A'B'$	6
	$A'B'A'$	$B'A'$	
	$B'A'A'$		
3	$A'A'A'B'B'$	$A'A'B'$	30
	$A'A'B'A'B'$	$A'B'A'$	
	$A'A'B'B'A'$	$B'A'A'$	
	$A'B'A'A'B'$		
	$A'B'A'B'A'$		
	$A'B'B'A'A'$		
	$B'A'A'A'B'$		
	$B'A'A'B'A'$		
	$B'A'B'A'A'$		
	$B'B'A'A'A'$		

on only the two values of the original Fibonacci tiling. All neighboring points are separated by either A or B, with $A/B = \tau$. Over a long range the ratio of the number of line segments of length A to the number of line segments of length B approaches $\tau:1$. Deflation of a one-dimensional quasiperiodic structure is a self-similar transformation that decomposes each line segment into smaller line segments, scaled down by a factor μ, which form a new quasiperiodic structure. In the cases considered here, $\mu = \tau^{-n}$ means that each line segment of length A is replaced by F_{n+1} line segments of length A' and F_n line segments of length B' and each line segment of length B is replaced by F_n line segments of length A' and F_{n-1} line segments of length B', where $F_n = [\tau^n - (-1/\tau)^n]/5^{1/2}$ are the Fibonacci numbers and $A' = \mu A$ and $B' = \mu B$. Thus, the scale factor μ determines only the number of line segments of lengths A' and B' and not their sequence within A and B. For $\mu = \tau^{-1}$, each A may be replaced by either the pair $A'B'$ or the pair $B'A'$ and each B is replaced by A'. Both possible combinations of deflated line segments, (1) $A \to A'B'$ and $B \to A'$ and (2) $A \to B'A'$ and $B \to A'$, yield the original Fibonacci tiling. For $\mu = \tau^{-2}$ there are three different ways to deflate A, namely $A'A'B'$, $A'B'A'$ and $B'A'A'$, and two different ways to deflate B, namely $A'B'$ and $B'A'$. For $\mu = \tau^{-3}$, there are ten different ways to deflate A and three different ways to deflate B. Table 1 gives the different deflation types of the line segments of lengths A and B for $\mu = \tau^{-n}$ with $1 \le n \le 3$. The 38 ($\mu = \tau^{-1}$: 2; $\mu = \tau^{-2}$: 6; $\mu = \tau^{-3}$: 30) combinations of the different deflation types result in nine different types of quasilattices (Table 2). The concept of local-isomorphism (LI) classes

Table 2. *The nine different types of quasilattice*

The first column gives the serial number of the types. Type 0 corresponds to the original Fibonacci tiling. The second column contains the different combinations of deflated line segments of lengths A and B, which yield quasilattices of the same type. The last column gives the width w of the atomic surface. $\alpha = \arctan(1/\tau)$ and $a = |\mathbf{a}_1| = |\mathbf{a}_2|$.

Type	Combinations of deflated line segments of lengths A and B	w
0	$A'B'+A'$, $B'A'+A'$, $A'A'B'+A'B'$, $A'B'A'+A'B'$, $A'B'A'+B'A'$, $B'A'A'+B'A'$, $A'A'B'A'B'+A'A'B'$, $A'B'A'A'B'+A'A'B'$, $A'B'A'A'B'+A'B'A'$, $A'B'A'B'A'+A'B'A'$, $B'A'A'B'A'+A'B'A'$, $B'A'B'A'A'+B'A'A'$	$a\tau\cos\alpha$ $\simeq 1.3764a$
1	$A'A'B'A'B'+A'B'A'$, $A'B'A'B'A'+A'A'B'$, $A'B'A'B'A'+B'A'A'$, $B'A'B'A'A'+A'B'A'$	$a\tau^3(\cos\alpha)/2$ $\simeq 1.8017a$
2	$B'A'A'A'B'+A'B'A'$	$a5^{1/2}\cos\alpha$ $\simeq 1.9021a$
3	$A'B'A'A'B'+B'A'A'$, $B'A'A'B'A'+A'A'B'$	$3a\tau(\cos\alpha)/2$ $\simeq 2.0646a$
4	$A'A'A'B'B'+A'A'B'$, $A'A'B'B'A'+A'A'B'$, $A'A'B'B'A'+A'B'A'$, $A'B'A'A'B'+A'B'A'$, $A'B'B'A'A'+B'A'A'$, $B'A'A'A'B'+A'A'B'$, $B'A'A'B'A'+B'A'A'$, $B'B'A'A'A'+B'A'A'$	$3a\tau(\cos\alpha)/2$ $\simeq 2.0646a$
5	$A'A'B'+B'A'$, $B'A'A'+A'B'$	$a\tau^2\cos\alpha$ $\simeq 2.2270a$
6	$A'A'B'A'B'+B'A'A'$, $B'A'B'A'A'+A'A'B'$	$a(3\tau+1)(\cos\alpha)/2$ $\simeq 2.4899a$
7	$A'A'A'B'B'+A'B'A'$, $A'A'B'B'A'+B'A'A'$, $A'B'B'A'A'+A'A'B'$, $B'B'A'A'A'+A'B'A'$	$a(3\tau+1)(\cos\alpha)/2$ $\simeq 2.4899a$
8	$A'A'A'B'B'+B'A'A'$, $B'B'A'A'A'+A'A'B'$	$a(4\tau+1)(\cos\alpha)/2$ $\simeq 3.1781a$

(Levine & Steinhardt, 1986; Socolar & Steinhardt, 1986) was used to subdivide the quasilattices generated by means of the 38 combinations of deflation types into different equivalence classes. The subdivision of the quasilattices into nine different types (LI classes) was achieved with use of the corresponding atomic surfaces. Their determination will be discussed in the next section.

The frequencies of interpoint distances calculated by substitution matrices (Mandelbrot, Gefen, Aharony & Peyrière, 1985; Olami & Kléman, 1989) of the nine different types of quasilattices are listed in Table 3, up to a maximum distance of $r = 5B$. One interesting feature of these new quasilattices is that there exist several types of quasilattices, which have the same frequencies of pairs, triplets, quadruplets, ... of adjacent line segments (Table 3) and differ only if one takes larger clusters of adjacent line segments into account. Comparable properties have been found in quasiperiodic pentagonal plane tilings (Zobetz, 1992).

3. Embedding methods

Although deflation procedures allow a fast and direct generation of a certain type of quasiperiodic structure and may be helpful to describe several properties by means of substitution matrices, by far the best way to derive the diffraction pattern of a quasicrystal is

Table 3. *Frequencies of interpoint distances that occur in the nine different types of quasilattices, up to a maximum distance of* $r = 5B$

The lower rows give the corresponding clusters of adjacent line segments.

					r/B					
	1	$\tau\simeq$	2	$1+\tau\simeq$	3	$2\tau\simeq$	$2+\tau\simeq$	$1+2\tau\simeq$	$3+\tau\simeq$	$3\tau\simeq$
Type	1.0000	1.6180	2.0000	2.6180	3.0000	3.2360	3.6180	4.2360	4.6180	4.8541
0	0.7639	1.2361	-	1.5279	-	0.4721	0.2918	1.7082	-	-
1	0.7639	1.2361	-	1.5279	-	0.4721	0.4721	1.3475	-	0.1803
2	0.7639	1.2361	0.1459	1.2361	-	0.6180	0.5836	1.1246	-	0.2918
3	0.7639	1.2361	0.1459	1.2361	-	0.6180	0.4377	1.4164	-	0.1459
4	0.7639	1.2361	0.2918	0.9443	-	0.7639	0.5836	1.1246	-	0.2918
5	0.7639	1.2361	0.2111	1.1056	-	0.6833	0.5029	1.2859	0.0807	0.2111
6	0.7639	1.2361	0.1459	1.2361	-	0.6180	0.5836	1.1246	0.1459	0.2918
7	0.7639	1.2361	0.2918	0.9443	-	0.7639	0.6950	0.9017	0.1115	0.4033
8	0.7639	1.2361	0.3820	0.7639	0.0902	0.8541	0.5836	0.8541	0.1803	0.4721
	B	*A*	*BB*	*AB*	*BBB*	*AA*	*ABB*	*AAB*	*ABBB*	*AAA*
				BA			*BAB*	*ABA*	*BABB*	
							BBA	*BAA*	*BBAB*	
									BBBA	

through the knowledge of either the window or the atomic surface. Appropriate embedding of a quasilattice into higher-dimensional space also has the advantage that the whole apparatus of crystallography is applicable in higher-dimensional space (Janner, 1991; Janssen, 1991, 1992).

Projection method. A one-dimensional quasilattice may be obtained by multiplication of a periodic two-dimensional lattice by a window function that has the value unity within the window and the value zero outside. The lattice points that lie within the window are projected onto physical space. The projected lattice points give a quasilattice if the slope of physical space is irrational with respect to the two-dimensional lattice, otherwise (rational slope) the projected lattice points yield a periodic lattice, where the period depends on the slope of physical space. The Fourier transform of the set of projected lattice points is a cut through the convolution of the Fourier transform of the two-dimensional lattice (which is just the set of reciprocal-lattice points of the two-dimensional lattice) and the Fourier transform of the window.

Section method. The condition that all lattice points of the two-dimensional lattice that lie within the window will be projected onto physical space may be reformulated as follows. The two-dimensional structure consists of line elements (atomic surfaces) perpendicular to physical space, attached to the nodes of the two-dimensional lattice. The intersections between the atomic surfaces and physical space define the positions of the quasilattice points. Since the two-dimensional structure may be considered as the convolution of the atomic surface with the two-dimensional lattice, its Fourier transform is the product of the transforms of the atomic surface and the lattice. Subsequent projection (the Fourier transform of a section corresponds to a projection and *vice versa*) onto physical space yields the Fourier transform of the quasilattice.

If an atomic surface and the cross section of a window perpendicular to physical space have the same shape, the two methods yield quasilattices of the same type. Therefore, we confine ourselves in the following to the section method.

Let $\mathbf{L}=\{\mathbf{t}\,|\,\mathbf{t}=n_1\mathbf{a}_1+n_2\mathbf{a}_2,\ n_i\in Z\}$ be a square lattice with the basis vectors $\mathbf{a}_1$ and $\mathbf{a}_2$ ($a=|\mathbf{a}_1|=|\mathbf{a}_2|$) in two-dimensional space $\mathbf{V}$. An orthogonal coordinate system with the axes denoted $\mathbf{X}_\parallel$ (physical space) and $\mathbf{X}_\perp$ (perpendicular space) is introduced that is an angle $\alpha=\arctan(1/\tau)$ counterclockwise from $\mathbf{a}_1$. The components $\mathbf{a}_\parallel$ and $\mathbf{a}_\perp$ of the basis vectors are obtained by use of the relations $\mathbf{a}_\parallel=\mathbf{P}_\parallel\mathbf{a}$ and $\mathbf{a}_\perp=\mathbf{P}_\perp\mathbf{a}$, where in the case of a square lattice the projection operators $\mathbf{P}_\parallel$ and $\mathbf{P}_\perp$ (Elser, 1986) are given by

$$\mathbf{P}_\parallel=\begin{pmatrix}\cos^2\alpha & \cos\alpha\sin\alpha\\ \cos\alpha\sin\alpha & \sin^2\alpha\end{pmatrix} \tag{3.1}$$

and

$$\mathbf{P}_\perp=\mathbf{I}-\mathbf{P}_\parallel=\begin{pmatrix}\sin^2\alpha & -\cos\alpha\sin\alpha\\ -\cos\alpha\sin\alpha & \cos^2\alpha\end{pmatrix}, \tag{3.2}$$

where $\mathbf{I}$ denotes the unit matrix. The position of a quasilattice point that is the intersection of an atomic surface $\Theta_\perp$ attached to the endpoint of a lattice vector $\mathbf{t}=n_1\mathbf{a}_1+n_2\mathbf{a}_2$ of the two-dimensional lattice with physical space $\mathbf{X}_\parallel$ is given by $\mathbf{t}_\parallel=n_1\mathbf{a}_{\parallel 1}+n_2\mathbf{a}_{\parallel 2}$. For the position vector of a lattice point projected onto perpendicular space $\mathbf{X}_\perp$, we find $\mathbf{t}_\perp=n_1\mathbf{a}_{\perp 1}+n_2\mathbf{a}_{\perp 2}$. The one-dimensional quasilattice is the set $\mathbf{L}_\parallel=\{\mathbf{t}_\parallel\,|\,\Theta_\perp * \mathbf{t}\cap\mathbf{X}_\parallel\neq\varnothing\}$, where the symbol $*$ represents the operation of convolution. The reciprocal two-dimensional square lattice is the set $\mathbf{L}^*=\{\mathbf{h}\,|\,\mathbf{h}=h_1\mathbf{a}_1^*+h_2\mathbf{a}_2^*,\ h_i\in Z\}$, where $\mathbf{a}_1^*$ and $\mathbf{a}_2^*$ are the reciprocal basis vectors and satisfy $\mathbf{a}_i\cdot\mathbf{a}_j^*=\delta_{ij}$. The components of $\mathbf{h}$ in physical and perpendicular reciprocal space are given by $\mathbf{h}_\parallel=h_1\mathbf{a}_{\parallel 1}^*+h_2\mathbf{a}_{\parallel 2}^*$ and $\mathbf{h}_\perp=h_1\mathbf{a}_{\perp 1}^*+h_2\mathbf{a}_{\perp 2}^*$, with $\mathbf{a}_{\parallel i}\cdot\mathbf{a}_{\parallel j}^*+\mathbf{a}_{\perp i}\cdot\mathbf{a}_{\perp j}^*=\delta_{ij}$.

To describe the shape of an atomic surface we introduce the function

$$S(\mathbf{x}_\perp)=\begin{cases}1 & \text{if } \mathbf{x}_\perp \in \Theta_\perp \\ 0 & \text{otherwise.}\end{cases} \tag{3.3}$$

In terms of the section method, the quasilattice $\mathbf{L}_\parallel$ is the intersection of $\mathbf{X}_\parallel$ with the convolution of the lattice $\mathbf{L}$ with $S(\mathbf{x}_\perp)$. Thus, the structure amplitude $F(\mathbf{h}_\parallel)$ of a reciprocal quasilattice point $\mathbf{h}_\parallel$ is given by

$$F(\mathbf{h}_\parallel)=S^*(\mathbf{h}_\perp)F(\mathbf{h}), \tag{3.4}$$

where $S^*(\mathbf{h}_\perp)$ denotes the Fourier transform of $S(\mathbf{x}_\perp)$ and $F(\mathbf{h})$ is the structure amplitude of the two-dimensional reciprocal-lattice point $\mathbf{h}$.

The atomic surfaces corresponding to the 38 possible combinations of deflated line segments were determined in the following way. For each type of quasilattice, about 500 000 points were generated in physical space $\mathbf{X}_\parallel$ by means of the corresponding deflation rules. Subsequently, these quasilattice points were embedded in the two-dimensional space $\mathbf{V}$ and projected onto perpendicular space $\mathbf{X}_\perp$ according to the relations described above. The maximum and minimum values of $\mathbf{t}_\perp$ determine the width $w=|\mathbf{t}_{\perp\max}-\mathbf{t}_{\perp\min}|$ of an atomic surface. In the case of the original Fibonacci quasilattice, the atomic surface has no discontinuities and its width is given by $w_0 = a\cos\alpha + a\sin\alpha$ (Elser, 1986). Widths greater than w_0 indicate disconnected atomic surfaces. The distribution function of projected lattice points of each atomic surface was divided into $n=2000$ strips of equal width $\Delta_w = w/n$. The normalized height of a strip is given by $v_j=[\mathbf{t}_\perp]_j/[\mathbf{t}_\perp]_{\max}$, where $[\mathbf{t}_\perp]_j$ is the number of projected lattice points that fall into the jth strip and $[\mathbf{t}_\perp]_{\max}$ is the maximum of the n $[\mathbf{t}_\perp]_j$. Deviations of v_j from 0 or 1 indicate that the jth strip consists of at least one region where $S(\mathbf{x}_\perp)=1$ and at least one region where $S(\mathbf{x}_\perp)=0$.†

Several deflation rules yield identical atomic surfaces. The nine different types of atomic surface are shown in Fig. 1. Since there is a one-to-one correspondence between the set $\mathbf{L}_\perp=\{\mathbf{t}_\perp\}$ and the set $\mathbf{L}_\parallel=\{\mathbf{t}_\parallel\}$, the subdivision into nine different types of atomic surfaces applies equally to the quasilattices (Table 2).

The atomic surfaces show the following properties:

(1) The width w of an atomic surface (Table 2) obviously depends on both the length and the frequency of periodic inclusions (*e.g.* *AA*, *AAA*, *AAAA*, ... or *BB*, *BBB*, ...).

(2) The small and large details of the atomic surfaces seem to be geometrically identical except for scale. This can best be seen for the atomic surface of type 2. Fig. 2 shows a magnification sequence of this atomic surface. Each successive figure represents a magnification of a selected portion of the previous figure up to a final magnification of more than 23. Each magnified portion is similar to the whole and to each other magnified portion. Objects for which each piece of the shape is geometrically similar to the whole are called self-similar, meaning that they remain 'similar' to themselves after a change of scale. This is not surprising, since the quasilattices have been generated by means of deflation rules, which are directly related to self-similarity. This property is trivially present in the original Fibonacci quasilattice (type 0), where the atomic surface is a line element without any discontinuities.

Thus, evidence suggests that the atomic surfaces are regular fractal objects. This suggestion has been

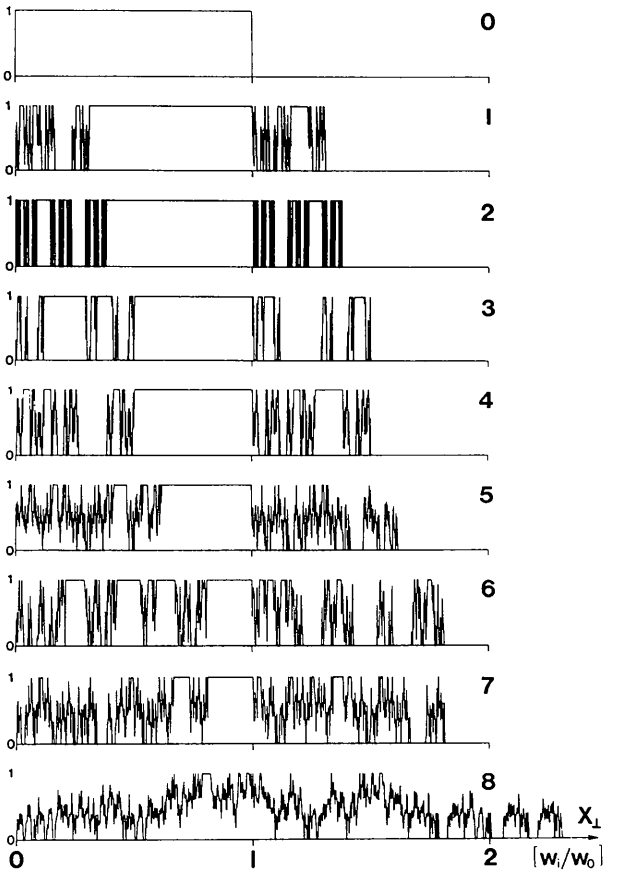

Fig. 1. Distribution functions (atomic surfaces) of the lattice points projected onto perpendicular space $\mathbf{X}_\perp$ [$S(\mathbf{x}_\perp)$ *versus* $\mathbf{x}_\perp$] of the nine different types of quasilattice. w_0 denotes the width of the atomic surface of the original Fibonacci quasilattice (type 0).

† Atomic surfaces divided into smaller strips ($n>2000$) could be obtained but would not alter the results substantially, although there would be less v_j differing significantly from 0 or 1. $n=2000$ was considered to be large enough, since the largest differences between the squared Fourier transforms (see § 4) of an atomic surface divided into $n=2000$ strips obtained by ~500 000 quasilattice points and an atomic surface divided into $n=4000$ strips obtained by ~1 000 000 quasilattice points in the range $|\mathbf{h}_\perp|=0$ to 30 ($a=1.0$ Å) were less than 0.003%; the mean deviations were less than 0.0003%.

confirmed by several properties of the quasilattices (*e.g.* frequencies of interpoint distances and squared Fourier transforms) that correspond to different stages of fractal development (see § 5) of the different types of atomic surface.

4. Fourier transforms and diffraction patterns

To derive the Fourier transform $S^*(\mathbf{h}_\perp)$ of an atomic surface $S(\mathbf{x}_\perp)$, each atomic surface was divided into $n = 2000$ strips of width $\Delta_w = w/n$. The Fourier transform of the jth ($j = 1$ to n) strip is given by

$$S^*(\mathbf{h}_\perp)_j = v_j \int_{l_j}^{u_j} \exp(2\pi i \mathbf{h}_\perp \cdot \mathbf{x}_\perp)\, \mathrm{d}x_\perp, \qquad (4.1)$$

where l_j and u_j denote the lower and upper bounds and v_j denotes the normalized height of the jth strip. The Fourier transforms of the n strips are added to give the total Fourier transform of the atomic surface,

$$S^*(\mathbf{h}_\perp = \sum_{j=1}^{n} S^*(\mathbf{h}_\perp)_j$$

$$= \sum_{j=1}^{n} v_j \int_{l_j}^{u_j} \exp(2\pi i \mathbf{h}_\perp \cdot \mathbf{x}_\perp)\, \mathrm{d}x_\perp. \qquad (4.2)$$

Integration and simple manipulations yield

$$S^*(\mathbf{h}_\perp) = (A + iB)(\sin\delta)/(\pi h_\perp), \qquad (4.3)$$

where

$$A = \sum_{j=1}^{n} v_j \cos(\alpha_j - \delta), \qquad B = \sum_{j=1}^{n} v_j \sin(\alpha_j - \delta),$$

$$\alpha_j = 2\pi h_\perp (j\Delta_w + l_1)$$

and

$$\delta = \pi h_\perp \Delta_w.$$

Fig. 3 shows the squared Fourier transforms, $|S^*(\mathbf{h}_\perp)|^2 = (A^2 + B^2)[(\sin\delta)/(\pi h_\perp)]^2$, of the nine different atomic surfaces. The squared Fourier transforms show three characteristic features:

(i) The points at which the functions fall to zero are the same for all nine functions and correspond to integer multiplies of $1/w_0$ ($w_0 = a\cos\alpha + a\sin\alpha$).

(ii) The half-widths of the maxima at $|\mathbf{h}_\perp| = 0$ decrease with increasing w.

(iii) It will be noticed that, in the squared Fourier transform of the atomic surface of type 0 (original Fibonacci quasilattice), the peak heights decrease monotonically with increasing $|\mathbf{h}_\perp|$. For example, there will be no intensities >1% of the central maximum with $|\mathbf{h}_\perp| > 2.68$ or >0.5% with $|\mathbf{h}_\perp| > 4.50$

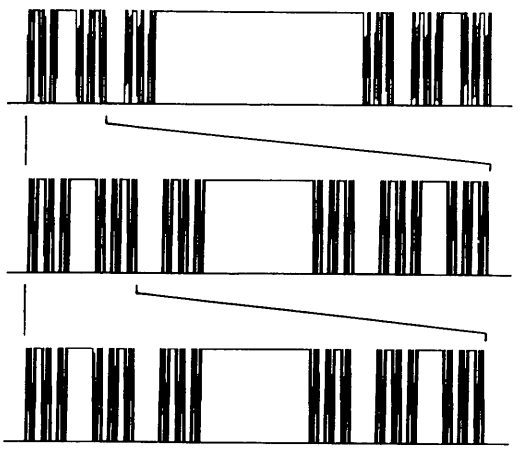

Fig. 2. Magnification sequence of the distribution function (atomic surface) of lattice points projected onto $\mathbf{X}_\perp$ of the quasilattice of type 2. Each successive figure represents a magnification of a selected portion of the previous figure up to a final magnification of more than 23.

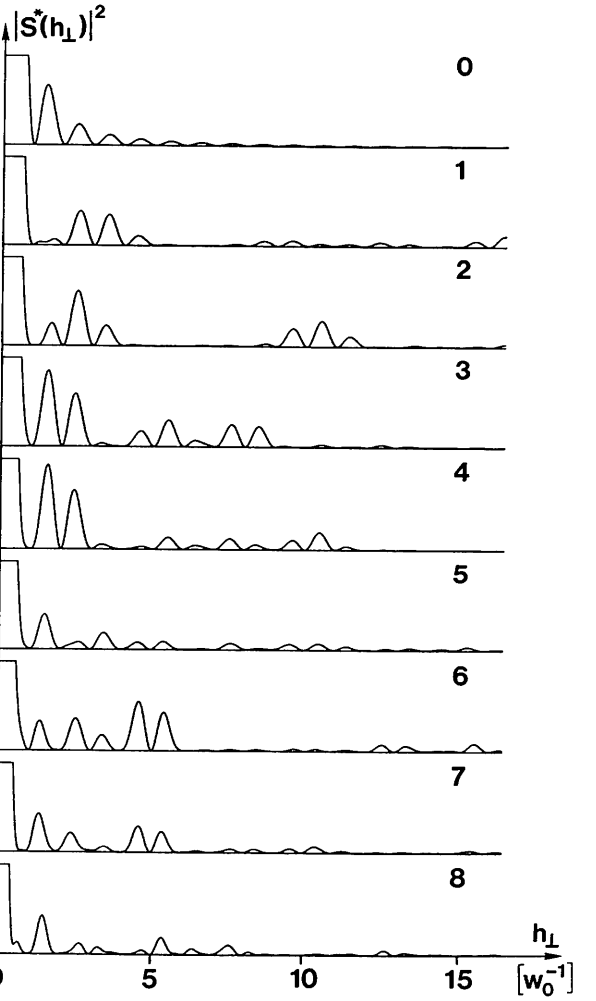

Fig. 3. The squared Fourier transforms of the nine different atomic surfaces. The curves are truncated at the 7% level of the central maximum at $\mathbf{h}_\perp = 0$.

($a = 1.0$). Since the distance between two reciprocal-lattice points in perpendicular space increases with decreasing distance in physical space and since we have only detection systems with a discrete minimum of detectable intensity, the diffraction pattern of the original Fibonacci quasilattice will consist of isolated Bragg peaks. In the Fourier transforms of the other quasilattices, the peak heights do not converge monotonically and as quickly to zero as in the squared Fourier transform of the original Fibonacci quasilattice. This may lead to diffraction patterns where reflections cannot be resolved and leave some uncertainties when the diffraction pattern is indexed, despite the fact that there always exists an uncertainty of a factor of τ^n.

Fig. 4 shows simulated diffraction patterns derived from the nine different atomic surfaces shown in Fig. 1. A single scattering point with unit weight has been placed at each point of the two-dimensional lattice. The peaks have Lorentzian shape, the width at half-maximum is $0.3°2\Theta$, $\lambda = 1.5418$ Å and $a = 10$ Å. Several features of the patterns are of note:

(i) The positions of the peaks are the same for all nine diffraction patterns but their intensities decrease and hence their detectable number reduces, which is in accordance with the fact that the widths of the central maxima of the squared Fourier transforms decrease with increasing width of the atomic surfaces.

(ii) For type 3 and type 4, we see that a certain number of peaks are broadened.

(iii) For type 7, we see that there is a certain amount of 'diffuse' scattering.

Observations (ii) and (iii) are caused by overlapping peaks because, in the simulated diffraction patterns of these quasilattices, reflections with relatively large components $\mathbf{h}_\perp$ also yield detectable intensities.

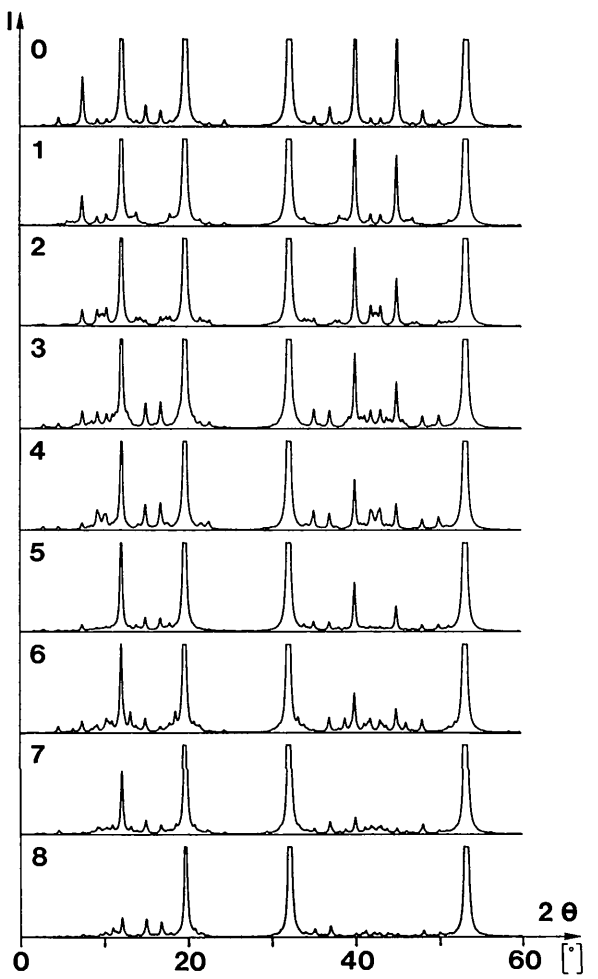

Fig. 4. Simulated diffraction patterns of the nine different types of quasilattices. The peaks have Lorentzian shape, the width at half-maximum is $0.3°2\Theta$, $\lambda = 1.5418$ Å and $a = 10$ Å. The peaks are truncated at the 20% level of $I(0, 0)$.

5. Fractal development of atomic surfaces

In the discussion in § 3 it was seen that the atomic surfaces obviously have self-similar properties; this indicated them to be fractally shaped objects (Mandelbrot, 1983). In the following, this observation will be explained by intuitive rather than rigorous arguments.

Construction methods for five of the eight fractally shaped atomic surfaces have been found, mainly by guesswork. The general procedure is as follows. One starts with the half-open interval $[r, s)$ as initiator. The two kinds of generator and the lengths of the intervals $d_1(n_f)$ and $d_2(n_f)$ depend on n_f, the stage of fractal development:

$n_f = 2n+1$:

$$[r - d_1(n_f), r), \quad [r + d_2(n_f), s - d_1(n_f)), \quad [s, s + d_2(n_f)); \tag{5.1}$$

$n_f = 2n$:

$$[r - d_2(n_f), r), \quad [r + d_1(n_f), s - d_2(n_f)), \quad [s, s + d_1(n_f)). \tag{5.2}$$

The initiator for each type of quasilattice is the half-open interval $[0, w_0)$. The atomic surface corresponding to the first fractal stage consists of three half-open intervals: $[-d_1(1), 0)$, $[d_2(1), w_0 - d_1(1))$ and $[w_0, w_0 + d_2(1))$. The first construction step is followed by application of the generator for $n_f = 2$, which yields nine half-open intervals:

$$[-d_1(1) - d_2(2), -d_1(1)),$$
$$[-d_1(1) + d_1(2), -d_2(2)), \quad [0, d_1(2)),$$
$$[d_2(1) - d_2(2), d_2(1)),$$
$$[d_2(1) + d_1(2), w_0 - d_1(1) - d_2(2)),$$

$$[w_0 - d_1(1),\ w_0 - d_1(1) + d_1(2)),\quad [w_0 - d_2(2),\ w_0),$$
$$[w_0 + d_1(2),\ w_0 + d_2(1) - d_2(2)),$$
$$[w_0 + d_2(1),\ w_0 + d_2(1) + d_1(2))$$

and so on *ad infinitum*. The values of $d_1(n_f)$ and $d_2(n_f)$ for the different types of atomic surface are listed in Table 4 and their effect on the initiator is shown in Fig. 5(*a*). The fractal development of the atomic surface of type 2 up to $n_f = 3$ is shown in Fig. 5(*b*).

The frequencies of interpoint distances (up to a maximum distance of $r = 5B$) of the quasilattices corresponding to the first three stages of fractal development of the atomic surface of type 2 are summarized in Table 5. They were calculated using the method introduced by Elser (1986). The values demonstrate convergence to the values derived by means of substitution matrices. This convergence has also been observed for the other types of quasilattices. The corresponding simulated diffraction patterns are shown in Fig. 6. They confirm the assumption that the atomic surfaces obtained by means of the deflation rules are the limits of decreasing approximations as the fractal atomic surfaces grow. The mean deviation between the squared Fourier transforms of the atomic surfaces after five steps of fractal development and the squared Fourier transforms of the atomic surfaces derived by means of the deflation procedure in the range $|\mathbf{h}_\perp| = 0$ to 30 ($a = 1.0$ Å) is for all types less

Table 4. *Generators for five of the nine different types of atomic surfaces*

n_f denotes the stage of fractal development. $\alpha = \arctan(1/\tau)$ and $a = |\mathbf{a}_1| = |\mathbf{a}_2|$.

Type	$d_1(n_f)$	$d_2(n_f)$
1	$a(\cos\alpha)/\tau^{3n_f}$	$a(\cos\alpha)/\tau^{3n_f+1}$
2	$a(\cos\alpha)/\tau^{3n_f}$	$a(\cos\alpha)/\tau^{3n_f}$
3	$2a(\cos\alpha)/\tau^{3n_f}$	$a(\cos\alpha)/\tau^{3n_f+1}$
4	$a(\cos\alpha)/\tau^{3n_f-1}$	$a(\cos\alpha)/\tau^{3n_f}$
5	$a(\cos\alpha)/\tau^{2n_f}$	$a(\cos\alpha)/\tau^{2n_f+1}$

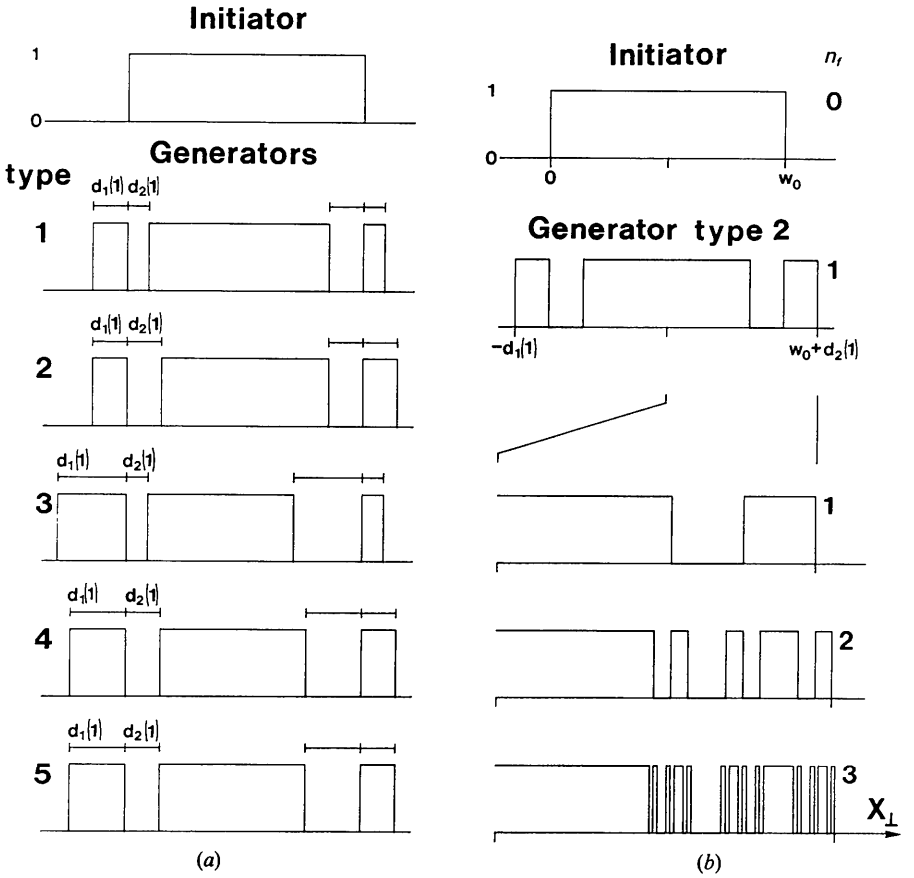

Fig. 5. Fractal generators and fractal development of the atomic surface functions $S(\mathbf{x}_\perp)$. (*a*) Initiator and generators of types 1–5. The atomic surfaces are shown after application of the first construction step. (*b*) Initiator, generator and the first three stages of fractal development of the atomic surface of type 2. n_f denotes the stage of fractal development. The fractal development is stopped at the limit of our eyes' resolution: the fourth stage would be indistinguishable from the last one (stage 3) depicted.

Table 5. *Frequencies of interpoint distances in the quasilattices corresponding to the fractal development of the atomic surface of type 2, up to a maximum distance of $r = 5B$*

n_f denotes the stage of fractal development. $n_f = 0$ corresponds to the original Fibonacci quasilattice (type 0) and $n_f = \infty$ to the quasilattice of type 2 obtained by means of the corresponding deflation rule. The last rows give the corresponding clusters of adjacent line segments.

						r/B				
	1	$\tau\simeq$	2	$1+\tau\simeq$	3	$2\tau\simeq$	$2+\tau\simeq$	$1+2\tau\simeq$	$3+\tau\simeq$	$3\tau\simeq$
n_f	1.0000	1.6180	2.0000	2.6180	3.0000	3.2360	3.6180	4.2360	4.6180	4.8541
0	0.7639	1.2361	-	1.5279	-	0.4721	0.2918	1.7082	-	-
1	0.7639	1.2361	0.1115	1.3050	-	0.5836	0.5836	1.1246	-	0.2918
2	0.7639	1.2361	0.1378	1.2523	-	0.6099	0.5836	1.1246	-	0.2918
3	0.7639	1.2361	0.1440	1.2399	-	0.6161	0.5836	1.1246	-	0.2918
⋮	⋮	⋮	⋮	⋮	⋮	⋮	⋮	⋮	⋮	⋮
∞	0.7639	1.2361	0.1459	1.2361	-	0.6180	0.5836	1.1246	-	0.2918
	B	*A*	*BB*	*AB*	*BBB*	*AA*	*ABB*	*AAB*	*ABBB*	*AAA*
				BA			*BAB*	*ABA*	*BABB*	
							BBA	*BAA*	*BBAB*	
									BBBA	

than 0.0003%; the maximum difference is for all types less than 0.002%.*

6. Homometric quasicrystals

A striking feature of the construction method for fractally shaped atomic surfaces is that generalization of this method yields infinitely many different atomic surfaces (and hence quasilattices) with the same squared Fourier transform. Structures that have the same diffraction pattern but that are neither congruent nor enantiomorphic are called homometric (Patterson, 1939). In the case of quasilattices, homometric structures belong to different LI classes. The cases where the two-dimensional structure is homometric are excluded here.

The Fourier transform of an atomic surface corresponding to a certain stage of fractal development and consisting of n half-open intervals is

$$S^*(\mathbf{h}_\perp) = \sum_{j=1}^{n} \int_{a_j}^{b_j} \exp(2\pi i \mathbf{h}_\perp \cdot \mathbf{x}_\perp)\, dx_\perp, \qquad (6.1)$$

where a_j and b_j denote the lower and upper bounds of the jth half-open interval. Integration yields

$$S^*(\mathbf{h}_\perp) = (B - iA)/2\pi h_\perp, \qquad (6.2)$$

where

$$A = \sum_{j=1}^{n} \cos 2\pi h_\perp b_j - \sum_{j=1}^{n} \cos 2\pi h_\perp a_j \qquad (6.3)$$

and

$$B = \sum_{j=1}^{n} \sin 2\pi h_\perp b_j - \sum_{j=1}^{n} \sin 2\pi h_\perp a_j. \qquad (6.4)$$

The squared Fourier transform is

$$|S^*(\mathbf{h}_\perp)|^2 = (A^2 + B^2)(2\pi h_\perp)^{-2}. \qquad (6.5)$$

Suppose there is a one-dimensional array of n points at positions $\mathbf{b}_j$ ($j = 1$ to n) with weights $w_b = +1$ and n points at positions $\mathbf{a}_j$ ($j = 1$ to n) with weights $w_a = -1$ in perpendicular space. The Fourier transform of this array is

$$F(\mathbf{h}_\perp) = w_b \sum_{j=1}^{n} \exp(2\pi i \mathbf{h}_\perp \cdot \mathbf{b}_j) + w_a \sum_{j=1}^{n} \exp(2\pi i \mathbf{h}_\perp \cdot \mathbf{a}_j)$$

* The largest differences between the squared Fourier transforms of the atomic surfaces of the fourth and fifth fractal stage derived by regular fractal development for each type of quasilattice were less than 0.0025%. The mean deviations were less than 0.0003%. The minimum length of an interval of the atomic surfaces corresponding to the 4th fractal stage is $a(\cos\alpha)/\tau^{13}$ [type 1 and type 3: $d_2(n_f) = a(\cos\alpha)/\tau^{3n_f+1}$], which corresponds approximately to $w/1250$.

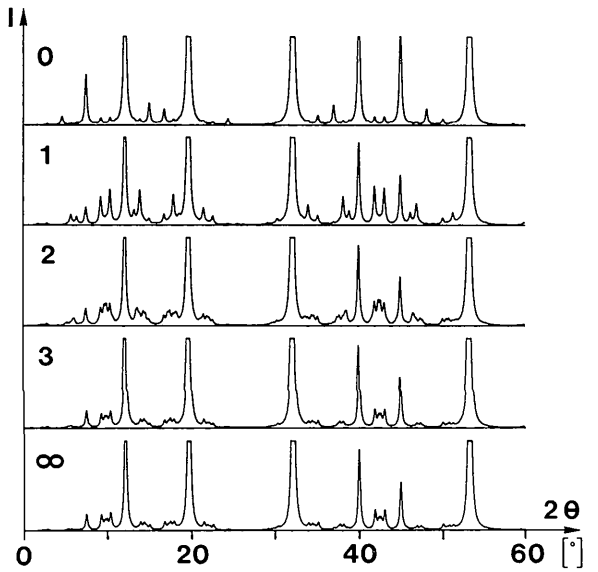

Fig. 6. Simulated diffraction patterns of the quasilattices corresponding to the fractal development of the atomic surface of type 2. The peaks have Lorentzian shape, the width at half-maximum is 0.3°2θ, $\lambda = 1.5418$ Å and $a = 10$ Å. The peaks are truncated at the 20% level of $I(0, 0)$.

$$= \sum_{j=1}^{n} \cos 2\pi h_\perp b_j - \sum_{j=1}^{n} \cos 2\pi h_\perp a_j + i\left(\sum_{j=1}^{n} \sin 2\pi h_\perp b_j - \sum_{j=1}^{n} \sin 2\pi h_\perp a_j \right). \quad (6.6)$$

If the endpoints of the vectors $\mathbf{a}_j$ and $\mathbf{b}_j$ correspond to the lower and upper bounds of the n half-open intervals of the atomic surface then, from (6.3) and (6.4), the Fourier transform of the one-dimensional array can be written as

$$F(\mathbf{h}_\perp) = A + iB \quad (6.7)$$

and the squared Fourier transform is given by

$$|F(\mathbf{h}_\perp)|^2 = A^2 + B^2. \quad (6.8)$$

Except for the factor $(2\pi h_\perp)^{-2}$, the squared Fourier transforms (6.5) and (6.8) are identical: $|F(\mathbf{h}_\perp)|^2 (2\pi h_\perp)^{-2} = |S^*(\mathbf{h}_\perp)|^2$. Thus, the initiator of an atomic surface may be defined in terms of a density distribution, ρ_I, that consists of two points with weights $w_a = -1$ and $w_b = +1$ separated by the distance w_0 (Fig. 7*a*). The density distributions of the generators, ρ_{nf}^+ (n_f odd) and ρ_{nf}^- (n_f even), consist of three points separated by the intervals with length $d_1(n_f)$ and $d_2(n_f)$ with weights w_b, w_a and w_b (Fig. 7*b*). $\rho^-(x)$ is a function that is symmetrical with the function $\rho^+(x)$ about the point $x = 0$, *i.e.* $\rho^-(x) = \rho^+(-x)$. The atomic surface of the first fractal stage (Fig. 7*c*), ρ_1, may be considered as the convolution of ρ_I with ρ_1^+, $\rho_1 = \rho_I * \rho_1^+$. $\rho_I * \rho_1^-$ is enantiomorphic to $\rho_I * \rho_1^+$.

An atomic surface after n_f steps of development can be expressed as

$$\rho_{nf} = \rho_I * \rho_1^+ * \rho_2^- * \rho_3^+ * \ldots * \rho_{nf}^+ \quad \text{for } n_f \text{ odd}$$

and

$$\rho_{nf} = \rho_I * \rho_1^+ * \rho_2^- * \rho_3^+ * \ldots * \rho_{nf}^- \quad \text{for } n_f \text{ even.}$$

It follows directly from the commutative law of convolution operations (Hosemann & Bagchi, 1954) that

$$\rho = \rho_1^\pm * \rho_2^\pm * \rho_3^\pm * \ldots * \rho_n^\pm$$

is a function with $2^{n'-1}$ homometric and $2^{n'-1}$ enantiomorphic forms, where n' denotes the number of asymmetric density distribution functions. Fig. 7(*d*) shows two homometric atomic surfaces, $\rho_I * \rho_1^+ * \rho_2^-$ and $\rho_I * \rho_1^+ * \rho_2^+$. They are enantiomorphic to $\rho_I * \rho_1^- * \rho_2^+$ and $\rho_I * \rho_1^- * \rho_2^-$, respectively. For $n_f = \infty$ (fractally shaped atomic surface), there exist infinitely many enantiomorphic and homometric atomic surfaces (quasilattices).

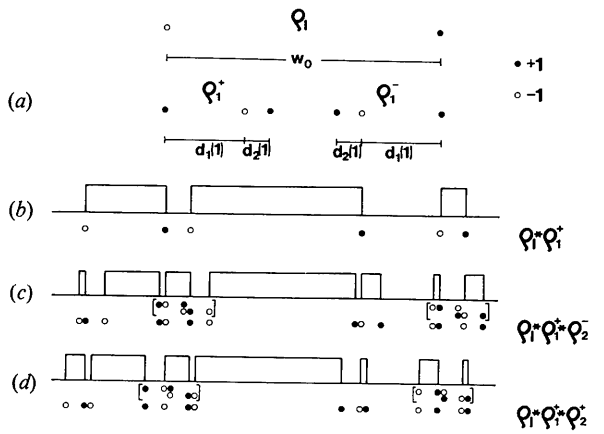

Fig. 7. Density distributions ρ and convolution products $*$. Solid circles represent points with weight $w_b = +1$, open circles points with weight $w_a = -1$. (*a*) Density distribution of the initiator, ρ_I, where $W_0 = a\cos\alpha + a\sin\alpha$. (*b*) Density distribution of the generators of type 2, $\rho_{n_f}^+$ and $\rho_{n_f}^-$. $d_1(n_f) = 2a(\cos\alpha)/\tau^{3n_f}$ and $d_2(n_f) = a(\cos\alpha)/\tau^{3n_f+1}$. (*c*) Convolution product $\rho_I * \rho_1^+$, which corresponds to the atomic surface of the first fractal stage. (*d*) Two homometric convolution products (atomic surfaces), $\rho_I * \rho_1^+ * \rho_2^-$ and $\rho_I * \rho_1^+ * \rho_2^+$. Since $d_1(n_f) = d_1(n_f + 1) + d_2(n_f + 1)$, two pairs of points with opposite weight come to lie at the same position. Therefore, the resulting density distribution consists of only 14 points instead of 18. The corresponding atomic surface consists of only seven instead of nine segments.

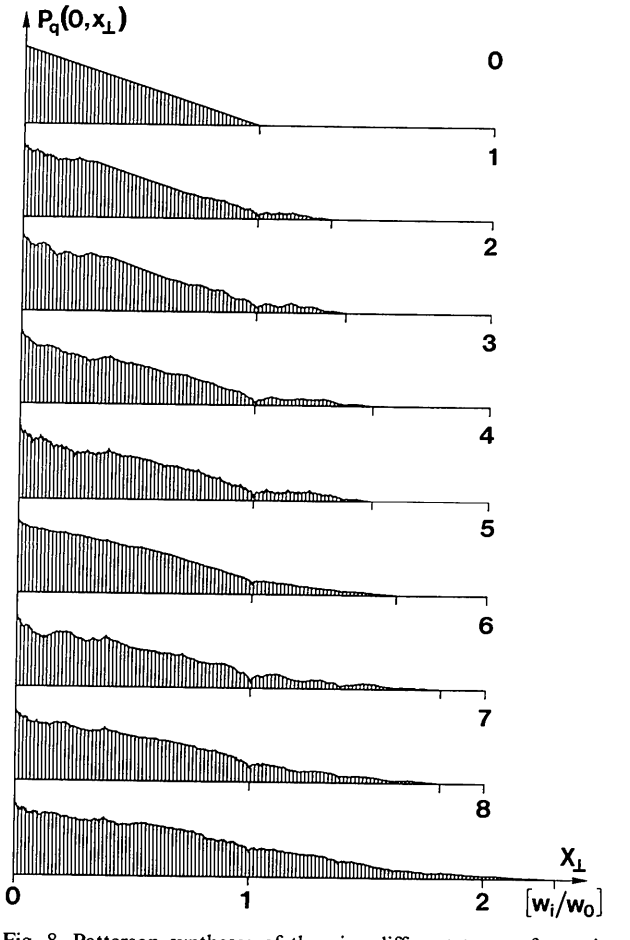

Fig. 8. Patterson syntheses of the nine different types of atomic surface along $\mathbf{X}_\perp$.

7. Structure determination

In the case of the original Fibonacci quasilattice, the width of the atomic surface can be obtained from the Patterson function $P_q(0, \mathbf{x}_\perp)$ along the perpendicular space $\mathbf{X}_\perp$. The Patterson function falls to a minimum as $|\mathbf{x}_\perp|$ increases from 0 to w_0. By means of the Fourier transform of this simple atomic surface,

$$S^*(\mathbf{h}_\perp) = \sin(\pi h_\perp w_0)/\pi h_\perp,$$

and according to (3.4), the $|F(\mathbf{h}_\parallel)|$ can be converted to $|F(\mathbf{h})|$. Direct methods are then used to solve the phase problem in two-dimensional space.

Fig. 8 shows the Patterson functions $P_q(0, \mathbf{x}_\perp)$ for the nine different types of quasilattice. Patterson functions with equal widths differ in their shape. To calculate $S^*(\mathbf{h}_\perp)$, one has to deconvolute the Patterson function to find the shape of the atomic surface. However, even if one allows rough approximations, it would be a tedious task to determine the shape of the atomic surfaces by means of the calculated Patterson functions, despite the fact that there exists an unlimited variety of homometric atomic surfaces.

References

BAK, P. (1986). *Phys. Rev. Lett.* **56**, 861–864.

BRUIJN, N. G. DE (1981). *K. Ned. Akad. Wet. Proc. Ser. A*, **43**, 39–66.

DIVINCENZO, D. P. (1986). *J. Phys. (Paris)*, **47**, C3, 237–243.

DUNEAU, M. & KATZ, A. (1985). *Phys. Rev. Lett.* **54**, 2688–2691.

ELSER, V. (1986). *Acta Cryst.* A**42**, 36–43.

GÄHLER, F. & RHYNER, J. (1986). *J. Phys. A*, **19**, 267–277.

HENLEY, C. L. (1986). *Phys. Rev. B*, **34**, 797–816.

HOSEMANN, R. & BAGCHI, S. N. (1954). *Acta Cryst.* **7**, 237–241.

JANNER, A. (1991). *Acta Cryst.* A**47**, 577–590.

JANSSEN, T. (1986). *Acta Cryst.* A**42**, 261–271.

JANSSEN, T. (1991). *Acta Cryst.* A**47**, 243–255.

JANSSEN, T. (1992). *Z. Kristallogr.* **198**, 17–32.

KALUGIN, P. A., KITAEV, A. Y. & LEVITOV, L. C. (1985). *J. Phys. (Paris) Lett.* **46**, L601–L607.

KOREPIN, V. E., GÄHLER, F. & RHYNER, J. (1988). *Acta Cryst.* A**44**, 667–672.

KRAMER, P. & NERI, R. (1984). *Acta Cryst.* A**40**, 580–587.

KUMAR, V., SAHOO, D. & ATHITHAN, G. (1986). *Phys. Rev. B*, **34**, 6924–6932.

LEVINE, D. & STEINHARDT, P. J. (1986). *Phys. Rev. B*, **34**, 596–616.

MANDELBROT, B. B. (1983). *The Fractal Geometry of Nature.* New York: Freeman.

MANDELBROT, B. B., GEFEN, Y., AHARONY, A. & PEYRIÈRE, J. (1985). *J. Phys. A*, **18**, 335–354.

OLAMI, Z. & KLÉMAN, M. (1989). *J. Phys. (Paris)*, **50**, 19–33.

PATTERSON, A. L. (1939). *Nature* (London), **143**, 939–940.

PENROSE, R. (1974). *Bull. Inst. Math. Appl.* **10**, 266–271.

PENROSE, R. (1979). *Math. Intell.* **2**, 32–37.

SHECHTMAN, D., BLECH, I., GRATIAS, D. & CAHN, J. W. (1984). *Phys. Rev. Lett.* **53**, 1951–1953.

SOCOLAR, J. E. S. (1989). *Phys. Rev. B*, **39**, 10519–10551.

SOCOLAR, J. E. S. & STEINHARDT, P. J. (1986). *Phys. Rev. B*, **34**, 617–647.

STEURER, W. (1990). *Z. Kristallogr.* **190**, 179–234.

ZIA, R. K. P. & DALLAS, W. J. (1985). *J. Phys. A*, **18**, L341–L345.

ZOBETZ, E. (1992). *Acta Cryst.* A**48**, 328–335.